Structural Engineering and Mechanics, *Vol. 48, No. 3 (2013) 309-331*
DOI: http://dx.doi.org/10.12989/sem.2013.48.3.309

A superelement formulation for efficient structural analysis in progressive collapse

Xu Long*, Weifeng Yuan, Kang Hai Tan and Chi King Lee

School of Civil and Environmental Engineering, Nanyang Technological University, 50 Nanyang Avenue, Singapore 639798, Singapore

(Received May 28, 2012, Revised August 30, 2013, Accepted October 20, 2013)

Abstract. An integrated superelement concept is proposed to improve the computational efficiency when analyzing structural responses during progressive collapses of large-scale structures, such as multi-storey reinforced concrete buildings. While the proposed methodology is straightforward and can be implemented into an existing finite element program with little effort, it is able to significantly reduce the computational cost without the loss of any critical information of the structural responses. Compared with the models without superelement, significant saving in computational cost and satisfactory prediction accuracy can be obtained with the proposed approach.

Keywords: superelement; computational efficiency; structural analysis; large-scale structures; progressive collapse

1. Introduction

The concept of superelement has been widely applied in efficient numerical simulations using finite element analysis. A superelement consists of a finite number of finite elements and is termed as a substructure as well. The idea was invented by aerospace engineers in the early 1960s to carry out a first-level breakdown of complex systems such as an entire airplane (Przemieniecki 1968). In the 1970s, the superelement technique as a new structural analysis method was incorporated in NASTRAN, a widely used finite element analysis solver, and the superelement technique started to be employed in practice. In order to test the superelement capability in NASTRAN, Zemer (1979) conducted quite extensive comparisons by using an aircraft model and proved that the superelement technique can result in substantial cost benefits for large scale structure analysis. To achieve a more versatile superelement technique, Jacobsen (1983) merged superelement/database concepts and summarized the advantages through the use of fully integrated superelements in basic finite element programs in terms of replication, reusability, matrix bandwidths, data generation, load condition, reanalysis and computational cost.

Due to the most attractive advantage to significantly improve computational efficiency, superelement method has been employed when solving various problems in recent years. The problem characteristics suitable for superelement applications can be summarized into three

*Corresponding author, Ph.D. Student, E-mail: LONG0026@e.ntu.edu.sg

http://www.techno-press.org/?journal=sem&subpage=8 ISSN: 1225-4568 (Print), 1598-6217 (Online)

distinguishing features, that is, iterative computational tasks, localized nonlinearity and a large number of finite elements in the numerical models for applications in dynamics.

Firstly, as for the iterative analysis and design in the topology optimization, superelement method can be adopted when a structure is locally designed for the topology optimization. Hence in a structure, the part outside the zone which is supposed to be locally optimized can be defined as a superelement and the corresponding stiffness remains the same in the later analysis, while only the stiffness matrix of the part within the optimized zone needs to be reformulated iteratively (Qiu *et al*. 2009).

Secondly, in the multibody problems, the large relative rotation between individual bodies introduces geometric nonlinearity in the computational model, while the deformation inside each body are small enough to be considered as elastic and, therefore, suitable for the superelement application (Cardona and Geradin 1991, Cardona 2000). Similarly, in the vehicle joints modelling (Maressa *et al*. 2011) the coupling interface between vehicle joints is the crucial region and can be defined as the connection between superelements.

Thirdly, for dynamic analysis, a large number of elements are needed to obtain accurate simulation results for the eigenvalue and frequency response. Thus, the idea of superelement can be utilized to decrease the model evaluation time by using a reduced model (Belyi 1993, Agrawal *et al*. 1994, De Gersem *et al*. 2007). Besides, the concept of superelement can also be easily implemented to condense a group of members or components with a superelement for large-scale structure analysis (Ju and Choo 2005, Steenbergen 2007, Belesis and Labeas 2010, Huang and Li 2010).

In addition to decreasing computational cost, the application of superelement provides the opportunity to overcome some modelling difficulties when tedious geometric details are involved in the models. For instance, in 3D seismic analysis of a high-rise building, due to the fine mesh around the shear wall with various types of openings, the degrees of freedom from the nodes which are not connected to beams and columns of interest will lead to unnecessary computational cost and they can be eliminated via the implementation of superelement before structural analysis commences (Kim *et al*. 2005).

Similar problems are also encountered in the present study on structural analysis for progressive collapse of buildings. It should be noted that the potential of progressive collapse of existing buildings has not been well researched previously and there was little research conducted except some technical reports until the collapse of the twin towers of World Trade Centre in September 2001 (National Institute of Standards and Technology 2005, Bazant and Verdure 2007, Yuan and Tan 2011). To check for progressive collapse, computational cost for nonlinear analysis of a large structure such as a multi-storey reinforced concrete (RC) building is always exorbitant since a large number of finite elements are needed to discretize the structure in order to obtain reasonably accurate predictions of the structural response (Hartmann *et al*. 2008). This is because although a relatively small portion of the building is initially subjected to extreme loads such as a blast event, it is required to simulate the response of the entire building with a time-consuming nonlinear model to ascertain whether the initial damage has spread to the other parts of the structure. Therefore, in practice, structural engineers often need to strike a balance between the computational cost employed and the accuracy in structural response predictions. It should be noted that modelling geometric and material nonlinearities using the finite element method requires almost always repeating updates of tangent stiffness matrix and solutions of the corresponding linear equation systems, which are the most time-consuming part in iterative numerical simulations. However, in many practical problems involving nonlinear analysis of large

structures such as the progressive collapses of multi-storey RC buildings, the material nonlinearity phenomena are usually localized in certain critical structural members (Unified Facilities Criteria (UFC)-DoD 2005) and might not dramatically spread throughout the whole structure even in the occurrence of progressive collapse. Thus, at each loading increment, the computational effort spent on the tangent stiffness matrix calculation and updating of structural members properties with only small deformation could be avoided using the concept of superelement.

The superelement formulation proposed in the present paper is vastly different from the conventional superelement formulation using static condensation (Wilson 1974) which is also known as Guyan reduction (Chen and Pan 1988). Firstly, in the conventional superelement formulation based on static condensation, many nodes in the mesh have to be renumbered, or the rows and the columns in the stiffness matrix have to be swapped to make the degrees of freedom (DOF) associated with the superelement to lie in the upper left sub-matrix in the system stiffness matrix. However, there is no such requirement in the superelement formulation proposed herein. This advantage of the proposed superelement formulation will further decrease the analysis time and, thus, benefit the objective to achieve efficient finite element analysis.

Secondly, material nonlinearity is the only concerned time-consuming part in finite element analysis of conventional superelement formulations based on static condensation. However, besides material nonlinearity, geometric nonlinearity can also be involved due to large rigid-body rotations when analyzing progressive collapse of structures. It should be noted that the structural regimes suitable for superelement applications are not always fixed on the foundation (or other essential boundary conditions) and do not always undergo small deformation. Actually, in general, there are two types of superelement configurations by differentiating whether the defined superelement is directly fixed onto the foundation. In many simulations regarding structural failures in the seismic events or terrorist bombing accidents, material nonlinearity is localized at the first storey of structures and the storeys above only undergo small deformation. Thus, the deformations of the storeys above the first are accompanied by large rigid-body rotations as shown in Fig. 1, which should be reasonably taken into account in the superelement formulation. However, in the conventional superelement formulations based on static condensation, the effect of superelement zone on the nonlinear zone is considered in the condensed stiffness matrix of the whole structure, and there is no independent explicit expression for the superelement stiffness matrix after the formation of superelement. Therefore, once the geometric nonlinearity needs to be taken into account for the superelement zone, the stiffness matrix of the whole structure has to be updated and this will considerably increase the computational cost.

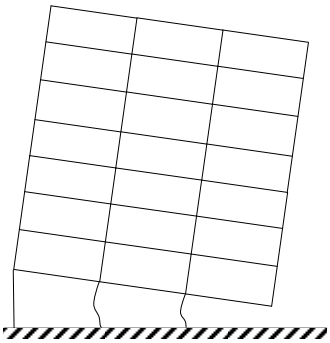

Fig. 1 A multi-storey building with a column removal at the first storey

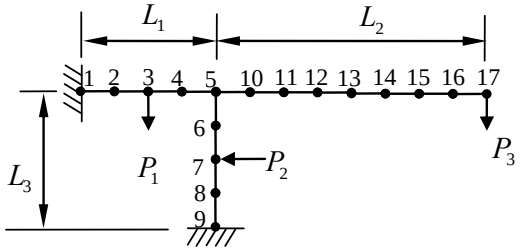

Fig. 2 A 2D frame subjected to external forces

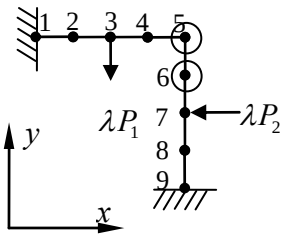

Fig. 3 Linear zone of the 2D frame under real forces

The outline of the present study is summarized as follows. In Section 2, the basic concept of the proposed superelement formulation is presented using a simple 2D frame example. The displacement of the superelement is discussed in detail for different superelement configurations in Section 3. Lastly, the proposed superelement formulation is validated against several examples with comparisons of prediction accuracy and CPU time for numerical models with and without superelement applications.

2. Basic concept of the proposed superelement

To illustrate the basic approach proposed in this paper, a 2D frame example as shown in Fig. 2 is considered. The frame is uniformly divided into eight three-node 3D beam elements, and three point loads are applied at nodes 3, 7 and 17, respectively. With the load P_3 at nodel 17 as the major load, it is assumed that in this example, greater attention should be paid on those key elements between node 5 and node 17 as nonlinear behaviours are expected to occur there. The zone comprising the key elements is denoted as a *nonlinear zone*. In this case, all the elements between node 1 and node 9 can be merged into one superelement or *linear zone* where only linear analysis is required.

Now consider the linear zone shown in Fig. 3, with the key elements and the force applied on them removed from the original model. To construct a superelement, its nodes must be determined from the beginning. The superelement deformation is the combination of deformations caused by (i) the external loads applied on the linear zone and (ii) the transferred internal forces from those common nodes along the boundary between the nonlinear zone and the linear zone. Thus, an additional node is necessary to represent the superelement deformation behaviour if there are external loads applied in the linear zone.

For the numerical model in Fig. 2, node 5 is the only common node shared by the nonlinear and the linear zones. Thus, the superelement has only two nodes, viz. common node 5 which has six degrees of freedom and an *additional node*, which is in the linear zone. Without loss of generality, node 6 is selected to be the *additional node*, in that there are external loads applied in the linear zone. To obtain the stiffness matrix of the superelement, a series of linear analyses has to be conducted based on the configuration shown in Fig. 3.

Firstly, forces λP_1 and λP_2, where λ is a nonzero factor defined as $1/(P_1^2+P_2^2)^{0.5}$ so as to be consistent with the applied load in the structural analysis, are applied to the linear zone and the associated deformations at node 6 and node 5 are calculated. The corresponding deformation vector induced by a combination of all scaled forces applied on the linear zones (λP_1 and λP_2 in

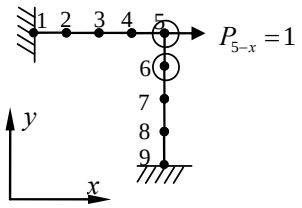

Fig. 4 Linear zone of the 2D frame under virtual force scenario

this example) is expressed as ${}^0\boldsymbol{U}=({}^0u_{6\text{-}x}, {}^0u_{5\text{-}x}, {}^0u_{5\text{-}y}, {}^0u_{5\text{-}z}, {}^0\theta_{5\text{-}x}, {}^0\theta_{5\text{-}y}, {}^0\theta_{5\text{-}z})^{\mathrm{T}}$ where superscript '0' indicates the load case number. Note that the terms u and θ represent the nodal displacements and rotations, respectively. The Arabic number in the subscript denotes the node number, while the Latin letter indicates the respective coordinate axis. It should be mentioned that all the six components of the deformation at node 5 are stored in ${}^0\boldsymbol{U}$ but only one degree of freedom at node 6 needs to be considered. In fact, among the six degrees of freedom at node 6, any nonzero component can be selected to form ${}^0\boldsymbol{U}$. In this method, the component with the maximum translation or rotation for load case '0' is selected as the additional component at the *additional node*.

Then, the applied loads in the linear zone are removed and a unit load is applied sequentially at all the degrees of freedom of the shared nodes by the linear and nonlinear zones. For this example, in the second step the forces λP_1 and λP_2 are removed and a unit load $P_{5\text{-}x}$ is applied to node 5 in x-direction as shown in Fig. 4. Similar to the first step, the deformations at node 6 and 5 are denoted as ${}^1\boldsymbol{U}=({}^1u_{6\text{-}x}, {}^1u_{5\text{-}x}, {}^1u_{5\text{-}y}, {}^1u_{5\text{-}z}, {}^1\theta_{5\text{-}x}, {}^1\theta_{5\text{-}y}, {}^1\theta_{5\text{-}z})^{\mathrm{T}}$.

The second step is repeated five times at the common node 5 to generate five more load cases, viz. two unit loads (along the y and z-axis) and three unit moments (about x, y and z-axis) are applied in sequence. The corresponding deformation vectors are stored as ${}^2\boldsymbol{U}, {}^3\boldsymbol{U}, {}^4\boldsymbol{U}, {}^5\boldsymbol{U}$ and ${}^6\boldsymbol{U}$. It should be mentioned that the global stiffness matrix of the linear zone only requires to be factorized once during such calculations. Hence, ${}^1\boldsymbol{U} \sim {}^6\boldsymbol{U}$ can be obtained with modest additional computational effort compared with the solution procedure of ${}^0\boldsymbol{U}$. Based on the properties of linear elasticity, the above three steps can be summarized by the following equation

$$\mathbf{K}_s\boldsymbol{\psi}=\begin{pmatrix}1 & \mathbf{0}_{1\times6}\\ \mathbf{0}_{6\times1} & \mathbf{I}_{6\times6}\end{pmatrix}_{7\times7}=\mathbf{I}_{7\times7} \tag{1}$$

where the displacement matrix $\boldsymbol{\psi}=({}^0\boldsymbol{U}, {}^1\boldsymbol{U}, {}^2\boldsymbol{U}, {}^3\boldsymbol{U}, {}^4\boldsymbol{U}, {}^5\boldsymbol{U}$ and ${}^6\boldsymbol{U})$ is obtained by conducting a series of linear analyses with consideration of the external loads in the linear zone (the forces λP_1 and λP_2 and the transferred internal forces from the common nodes (the assumed unit load cases applied to all degrees of freedom of node 5) and $\mathbf{K}_s$ is the superelement stiffness matrix and is equal to $\boldsymbol{\psi}^{-1}$, since the multiplication of $\mathbf{K}_s$ and the displacement matrix $\boldsymbol{\psi}$ is equal to the applied loads. The identity matrix is denoted by $\mathbf{I}$ in Eq. (1). In this example, the superelement has seven DOFs, including six DOFs at node 5 and only one DOF at node 6.

3. Superelement displacement

During a progressive collapse analysis of an RC building, based on the structural deformation

behaviour and the material states at different parts of the structure, the whole structure can be divided into two regions. The first is the linear elastic region where the nonlinear material effect is negligible so that the stiffness matrix does not change due to material nonlinearity and can be simulated by a superelement. The other is the nonlinear region where significant amount of nonlinear structural responses occur and the effects have to be solved by iterative computations in which the tangential stiffness matrix for this region will be updated as deformations increase.

In general, two types of superelement can be constructed. The first type of superelement is connected to both the nonlinear zone and the foundation (or where essential boundary conditions are specified). The second type of superelement is only connected to the nonlinear zone. For the first type of superelement the whole structure is partitioned into superelement and non-superelement zone as shown in Fig. 5. In this case, a direct amplification of the deformation in the superelement can be applied as follows. Large rigid-body rotation will be prevented by the foundations. The tangential stiffness matrix of this type of superelement will remain the same throughout the loading history. Therefore, the superelement stiffness matrix is only computed once before the iteration starts. To calculate the superelement deformations, after each converged increment is achieved, the nodal force vector at the common nodes (along the boundary between the superelement and the nonlinear zone) is applied as external loads to the superelement as shown in Fig. 6. Meanwhile, the deformation calculation of the superelement takes into account the nonlinear effects due to the nonlinear zone.

For the second type of superelement which is only connected to the nonlinear zone such as the framed structure shown in Fig. 7, '*weak member method*', which assigns a relatively small value to the material properties (e.g. both Young's modulus and shear modulus) for elements that are in the nonlinear zone, is employed to calculate the stiffness matrix of the superelement without the restraint of the foundation. In addition, '*strong member method*', which assigns a relatively larger value to the material properties for elements that are in the nonlinear zone, is employed to eliminate the nonlinear effect from the nonlinear zone when calculating the relative deformations of the superelement for the initial load factor. With the assumption that the superelement zone remains elastic, the global deformations can be obtained by combining the relative deformations and the rotation of the nonlinear zone.

It should be noted that only the relative deformations of the superelement zone (with respect to the nonlinear zone) show linear relationship with external loads in the superelement zone. In addition, the effects of nonlinear behaviour of the nonlinear zone on the superelement can be taken

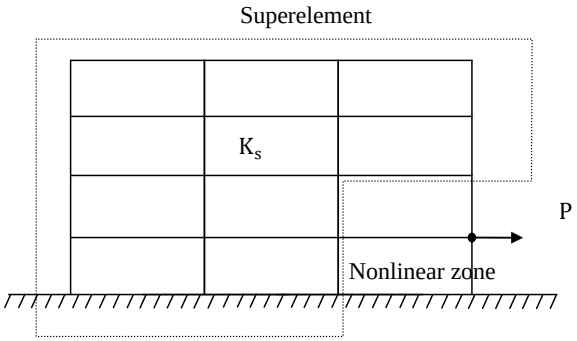

Fig. 5 First type of superelement

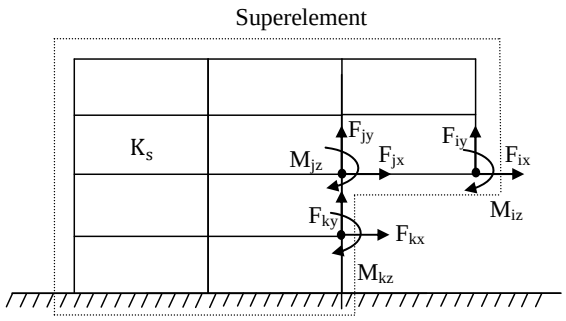

Fig. 6 The equivalent loading for superelement

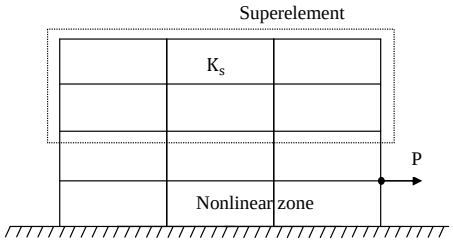

Fig. 7 Second type of superelement

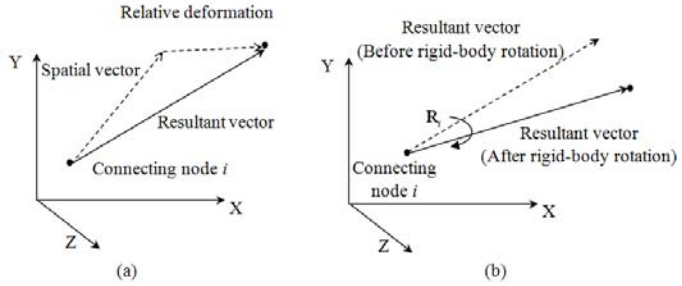

Fig. 8 Deformed configuration of a node of the superelement

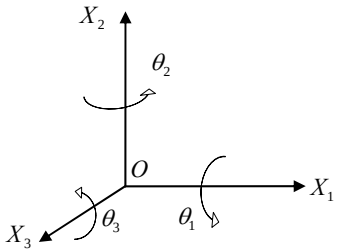

Fig. 9 Rotation directions defined by the skew-symmetric matrix

into account when calculating the rigid-body rotation which can be conducted with respect to certain connecting nodes as shown in Fig. 8. In Fig. 8(a), the resultant vector of a certain node within the superelement can be captured by the addition of the spatial vector (pointing from the interested node to the concerned node in the undeformed configuration) and the relative deformation. To take into consideration the effect of rigid-body rotation as discussed in Fig. 1 due to rotational deformation at the connecting node, the rotation matrix **R** will be employed to rotate the resultant vector with respect to the connecting node to the actual position in the deformed configuration, as shown in Fig. 8(b).

A conventional approach to calculate the rotation matrix proposed by Crisfield (1990) (relevant to Argyris' work (1982) dealing with 3D rotations) is to employ pseudo-vectors and skew-symmetric matrices to describe the rotational variables. Incorporating both local and global coordinate systems, the skew-symmetric matrix can be obtained as

$$\mathbf{S}(\theta)=\begin{bmatrix} 0 & -\theta_3 & \theta_2 \\ \theta_3 & 0 & -\theta_1 \\ -\theta_2 & \theta_1 & 0 \end{bmatrix} \tag{2}$$

where θ_1, θ_2, θ_3 are the natural rotational variables of the connecting node. The sign convention of rotational variables follows the right-hand rule as shown in Fig. 9.

The orthogonal rotation matrix **R** that rotates a vector into a new position is given by Argyris (1982) and Crisfield (1990).

$$\mathbf{R}(\boldsymbol{\theta})=\mathbf{I}+\frac{\sin\theta}{\theta}\mathbf{S}(\boldsymbol{\theta})+\frac{1\text{-}\cos\theta}{\theta^2}\mathbf{S}(\boldsymbol{\theta})\mathbf{S}(\boldsymbol{\theta}) \tag{3}$$

where $\boldsymbol{\theta}=(\theta_1\ \theta_2\ \theta_3)^T$ and $\theta=\|\boldsymbol{\theta}\|$. It should be noted that $\|\ \|$ represents the L_2-norm of a vector.

Another approach to calculate the rigid-body rotation about a certain node is based on the nodal vector in the deformed configuration as discussed by Crisfield (1996).

$$\mathbf{R}=\begin{bmatrix}\mathbf{e}_x & \mathbf{e}_y & \mathbf{e}_z\end{bmatrix} \tag{4}$$

where $\mathbf{e}_x$, $\mathbf{e}_y$, $\mathbf{e}_z$ are the unit local nodal vectors of the connecting node expressed in the global system.

Since it is well known that the definitions of rotation variables depend on the large rotational formulation of the finite element employed in the analysis (Dvorkin *et al*. 1988, Li 2007, Long *et al*. 2012), both approaches using Eqs. (3) and (4) have been implemented in the current study in order to broaden the application range of the proposed superelement to different finite element formulations, such as the total Lagrangian formulation, the updated Lagrangian formulation and the co-rotational formulation. For example, the first approach using natural rotation to define **R** (Eq. (3)) can be directly used with the 3D total Lagrangian beam element suggested by Dvorkin *et al*. (1988). However, if vectorial rotational vectors are employed to define the rotational variables (Li 2007, Long *et al*. 2012), it will be more convenient to use the second approach (Eq. (4)).

Rigid-body rotation and scalable relative deformation with respect to the nonlinear zone are computed to obtain the deformed configuration of the superelement in the global coordinate system. The computation procedure with superelement deformation is summarized in Fig. 10. Firstly, the superelement stiffness matrix $\mathbf{K}_s$ and its inverse matrix $\mathbf{K}_s^{-1}$ are calculated using the 'weak member method' and the 'strong member method' prior to the deformation predictions subjected to the total loading condition (Fig. 10(a)). Then as shown in Fig. 10(b), the relative deformation $\boldsymbol{u}_L$ of the superelement with respect to the nonlinear zone due to nodal force **F**, nodal moment **M** and external load $\mathbf{P}_s$ (including gravity load) within the superelement zone can be computed from Eq. (5).

$$\mathbf{u}_L=\mathbf{K}_s^{-1}\begin{pmatrix}\mathbf{P}_s\\ \mathbf{F}\\ \mathbf{M}\end{pmatrix} \tag{5}$$

It should be noted that the additional node and its degree of freedom have been considered when calculating the stiffness matrix $\mathbf{K}_s$ in Eq. (5). Therefore, in the relative deformation vector $\boldsymbol{u}_L$ there will be a relative deformation of the additional degree of freedom with respect to the nonlinear zone.

Assuming that the natural rotational variable (Eqs. (2) and (3)) are employed for large rotation formulation, then the rotation variables of connecting nodes are available to form the rigid-body rotation matrix **R** so that $\mathbf{R}^T=\mathbf{R}^{-1}$. Hence, the transformation matrix **T** can be obtained by assembling $\mathbf{R}^T$ corresponding to both the translational and rotational variables and the update of superelement stiffness matrix $\mathbf{K}_s$ can be calculated as

$$\mathbf{K}_s^{update}=\mathbf{T}^T\ \mathbf{K}_s\mathbf{T} \tag{6}$$

As illustrated in Fig. 10(c), after the convergence of the next load increment is reached and the updated superelement stiffness matrix $\mathbf{K}_s$ and the nonlinear zone stiffness matrix $\mathbf{K}_{ns}$ are

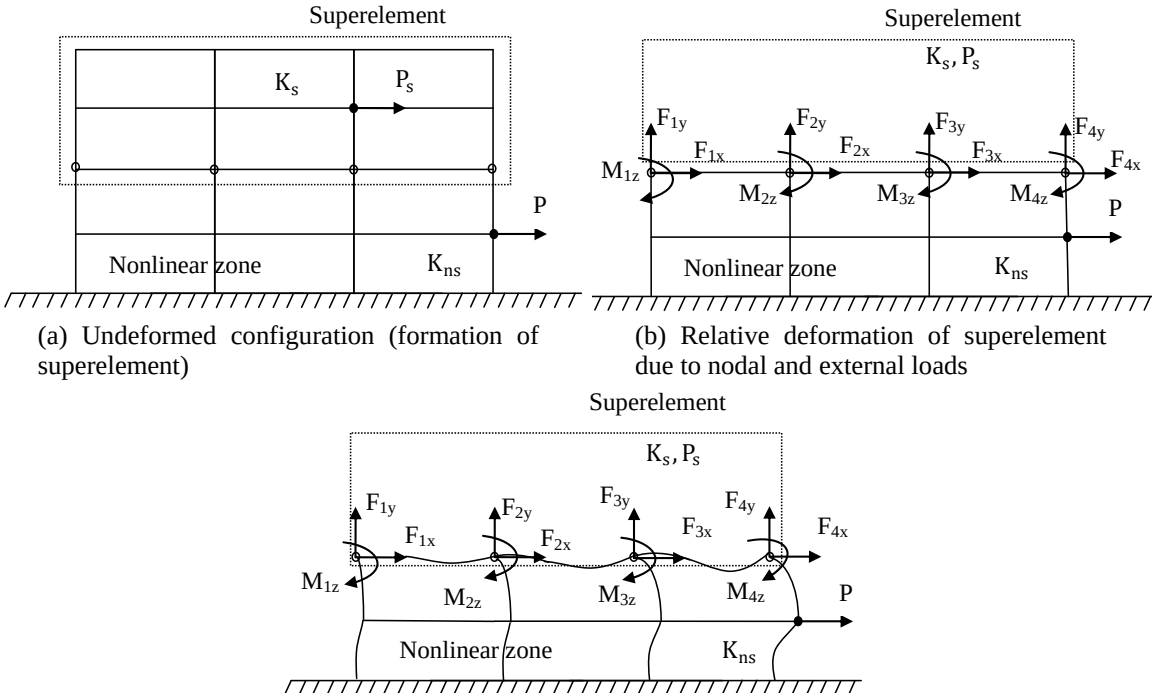

(a) Undeformed configuration (formation of superelement)

(b) Relative deformation of superelement due to nodal and external loads

(c) Global deformation of superelement zone and nonlinear zone

Fig. 10 Scalable relative deformation and rigid-body rotation with respect to the nonlinear zone

computed, the rotation variables of connecting nodes can be extracted to form the new rigid-body rotation matrix **R**. Therefore, the superelement deformation $\boldsymbol{u}_G$ for the next load increment in the global coordinate system can be calculated as

$$\mathbf{u}_G = \mathbf{R}\ \mathbf{u}_L \tag{7}$$

It should be pointed out that in the case of multi-connecting nodes, the formation of resultant rigid-body rotation matrix **R** of the superelement is approximated based on the 'average' of the rigid-body rotation matrix $\mathbf{R}_i$ at each connecting node. For the first approach using the natural rotation, it is apparent that the rotation matrix formulation in Eq. (3) is not additive due to the non-vectorial property of the 3D natural rotation. Therefore, the resultant of rotation matrices should be obtained based on compound rotations. As discussed by Crisfield (1990), one should first calculate the pseudo-vector $\boldsymbol{\omega}$ of the natural rotation at each connecting node, as given in Eq. (8)

$$\boldsymbol{\omega} = \frac{\tan(\theta/2)}{\theta/2}\boldsymbol{\theta} \tag{8}$$

Then the compound pseudo-vector for all connecting nodes can be computed. For example, $\boldsymbol{\omega}_{ij}$ is the compound pseudo-vector for connecting nodes *i* and *j* and can be expressed as

$$\boldsymbol{\omega}_{ij} = \frac{\boldsymbol{\omega}_i + \boldsymbol{\omega}_j - \frac{1}{2}\boldsymbol{\omega}_i \times \boldsymbol{\omega}_j}{1 - \frac{1}{4}\boldsymbol{\omega}_i^{\mathrm{T}}\boldsymbol{\omega}_j} \tag{9}$$

Lastly, the resultant rigid-body rotation matrix $\mathbf{R}(\boldsymbol{\omega}_{ij})$ of the superelement can be formed (Eq. (3)).

Compared with the first approach, the second approach using local nodal vectors to form the rotation matrix in Eq. (4) can be implemented more conveniently because of the additive property of the nodal vectors. Thus, the direct average of rigid-body rotation matrices $\mathbf{R}_i$ at connecting nodes can be treated as the resultant rigid-body rotation matrix $\mathbf{R}$ of the superelement.

The calculations for the superelement deformation are summarized for both types of superelement in a flow chart as shown in Fig. 11. For the situation of a superelement fixed onto the foundation, a direct amplification of the deformation of the superelement is conducted with reference to load factor (the ratio of the current applied load with respect to the maximum load intended to apply). For the situation of a superelement connected to other structural members and not directly fixed to the foundation, the present work proposes the concept of 'strong member method' in the superelement zone to recover the deformation of superelement zone. The formulation concerning the superelement zone with large displacement and large rotation in the 3D space is presented for different definitions of the rotational variables. The stiffness matrix in the superelement zone can be efficiently updated or kept constant as calculated in the undeformed configuration, respectively, depending whether the simulations emphasize accuracy or efficiency as the priority. The calculation of superelement deformation will be conducted with respect to the connecting node(s) and will avoid intensive computations on members which only undergo small linear deformations.

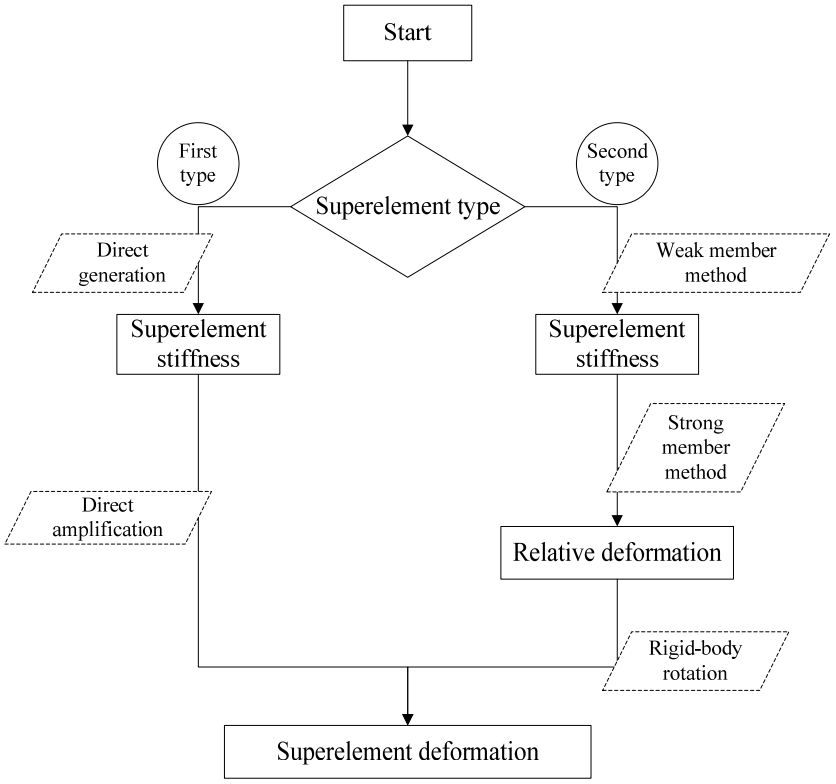

Fig. 11 Flow chart of the calculations for the superelement deformation

4. Numerical examples

The proposed superelement technique is implemented into a self-developed finite element package FEMFAN3D in NTU, Singapore. To validate the accuracy and effectiveness of the proposed superelement formulation, five examples including first and second types of the superelement are employed. Examples involving either elastic material or elasto-plastic material are compared with the theoretical solutions or numerical results obtained from full nonlinear analyses. Two examples of 3D beam-column steel frames and one example of a 2D reinforced concrete frame are employed to validate the accuracy of the superelement formulation in analyzing progressive collapse. In addition, the CPU time needed to complete the analyses with or without superelement are compared to study the efficiency of the superelement formulation. All the examples presented in this paper were simulated on the same computer with 2.66 GHz processor and 3.25 GB RAM.

It should be noted that an accurate and efficient finite element formulation is a prerequisite for the successful application of the proposed superelement formulation for progressive collapse analysis of structures. In the present work, the 3D three-node beam element with fibre model proposed by Long *et al*. (2012) was employed. In all the examples, the stiffness matrices of the superelement zone were kept constant and were calculated based on the original configuration. However, for the examples shown in this paper, it should be remarked here that further simulations using updated superelement stiffness matrix gave little changes in the calculation accuracy of nonlinear zone. In the first example where linear material properties were used, a simple four-fibre scheme was utilized to discretize the beam cross-section (Long *et al*. 2012), while more detailed fibre schemes were used for Examples 2, 3, 4 and 5 to capture more detailed stress and strain information such as yielding of steel fibres. For all of the examples employed in the present work, single-point integration was applied to each fibre and reduced integration procedure with two Gaussian points along the beam longitudinal axis was adopted.

Example 1: a cantilever beam with a concentrated load at the free end

A cantilever beam with length L=3.0 was employed as shown in Fig. 12 to demonstrate the feasibility of the proposed methodology to deal with superelement deformation. The cross-sectional dimension of the beam is 0.3×0.3. Young's modulus and Poisson's ratio are 2.1×10^{11} and 0.3, respectively. Since in this example linear elastic material is involved with small deformation, the load control method was utilized to increase the magnitude of the load P applied at the free end in 10 steps with a load increment equal to 10^5. Two three-node co-rotational beam elements were employed to discretize the cantilever beam as shown in Fig. 12. From the beam bending theory, the theoretical solution for the vertical displacement profile of the beam can be expressed as $Px^2(3L\text{-}x)/(6EI)$, where x is the distance of the point of interest to the fixed support.

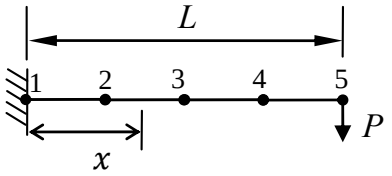

Fig. 12 Example 1: a cantilever beam with a concentrated load at the free end

Both first type and second type superelements were considered in this example. Firstly, the element with nodes 1, 2 and 3 was employed to define a superelement. Hence, there is no rigid-body movement for the superelement and the corresponding deformation is shown in Fig. 13(a). Secondly, the element with nodes 3, 4 and 5 was employed to define a superelement and the corresponding deformation obtained is shown in Fig. 13(b).

As shown in Figs. 13(a) and (b), the proposed formulation produced the exact theoretical solution no matter where the superelement was defined. It should be noted that the computational time was 6.61 s and 6.98 s for the models with superelement at the fixed end and the free end, respectively. The computational time needed for the model without superelement was 10.89 s. Therefore, a reduction of about 40% in computational time was achieved in this example.

To illustrate the improvement of computational efficiency in more detail, CPU time comparison for the models with and without superelement against 100 load increments is given in Fig. 14. Since the formation of the superelement was conducted at the beginning of the program, the total CPU time needed for the modelling with superelement was larger than that without superelement in the first few load increments. However, the efficiency of models with

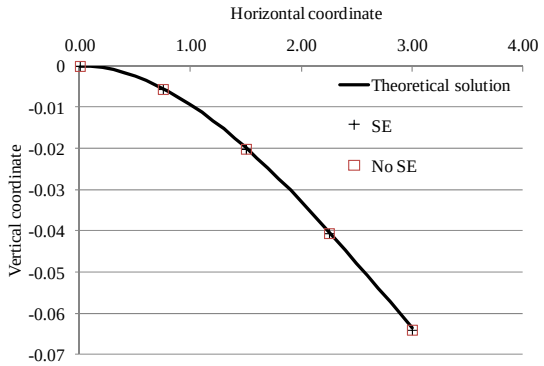

(a) Result comparisons for Example 1 with a superelement at the fixed support

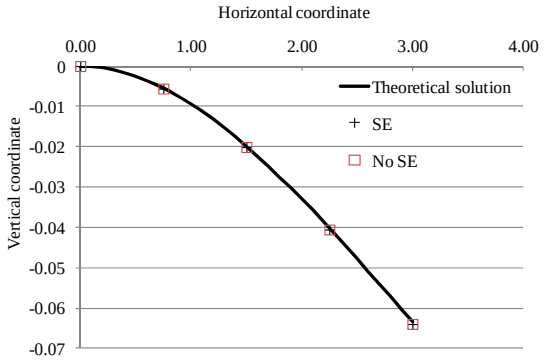

(b) Result comparisons for Example 1 with a superelement at the free end

Fig. 13 Result comparisons for Example 1

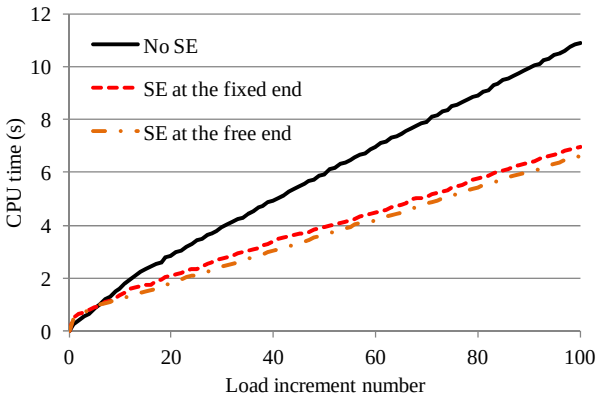

Fig. 14 CPU time comparison for Example 1 with and without superelement

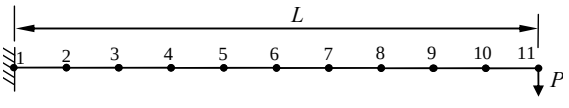

Fig. 15 The cantilever beam discretized by five beam elements

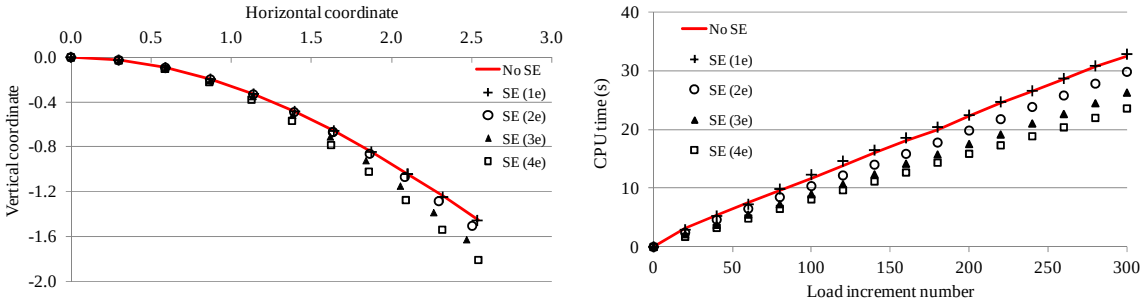

(a) Deformation (b) CPU time

Fig. 16 Comparison of the cantilevers with and without superelement

superelement increased as the numbers of load increments applied increased, because the saving in linear equations solution time gradually offset the CPU time needed for forming and factorizing the superelement in the first step.

To confirm that the current approach is reliable with relatively large rigid-body rotation of superelement under small deformation (which is quite common in the scenario of progressive collapse applications), five elements were employed to discretize the same cantilever beam as shown in Fig. 15. In this model, the effects of different sizes of the superelement zone were investigated. As shown in Fig. 16, the superelement zones consisting of one, two, three and four CR beam elements from the free end are denoted as 'SE (1e)', 'SE (2e)', 'SE (3e)' and 'SE (4e)', respectively. When the load applied at the free end was equal to 3×10^7 (the load factor is equal to $3\times10^7/10^5=300$), the results with and without superelement were compared and a good agreement between these simulations was achieved as illustrated in Fig. 16(a). Hence, the proposed superelement formulation can accurately predict the large rigid-body rotation of superelement with small deformation.

It should be noted that with increasing the number of elements in the superelement, the prediction accuracy is reduced, but the computational was more efficient as shown in Fig. 16(b).

Example 2: a 3D two-storey frame with material yield and failure at the first storey

To demonstrate the capacity of superelement to simulate responses of 3D structures consisting of elasto-perfectly plastic material, a two-storey beam-column frame with different cross-sectional shapes is employed as shown in Fig. 17(a). A similar one-storey frame had been analyzed by Marino (1970), Yang and Fan (1988), Gendy and Saleeb (1993) based on different approaches. The two-storey frame is validated against published results (Marino 1970, Yang and Fan 1988, Gendy and Saleeb 1993), because the applied loading and material yielding points are located at the first storey and the second storey only undergoes through a rigid-body movement if the plastic zone is localized in the first storey.

The columns and beams of the frame are made of W10×60 and W18×60 sections, respectively. The material properties are E=30,000 ksi (206.9 GPa), G=11,500 ksi (79.3 GPa), and σ_y=34 ksi (234.48 MPa). Each member is of length L=144 in (3.655 m) with warping restrained at both ends. All members were discretized by using eight beam elements and the cross-section orientations and fibre discretization are illustrated in Fig. 17(b).

Firstly, the numerical analysis without superelement was conducted and the corresponding

result is compared with the available simulation results (Marino 1970, Yang and Fan 1988, Gendy and Saleeb 1993). As shown in Fig. 18, the fibre model beam elements employed (Long *et al*. 2012) produced satisfactory prediction for the two-storey frame subjected to external loads. Then the numerical model with all elements at the second storey defined as a superelement was employed and compared with the full model without superelement. The deformation and the displacement versus loading curves obtained are shown in Figs. 19 and 20, respectively. To achieve an 8-inch deformation in the Z direction at node 2, a comparison of CPU time needed to complete the analysis is presented in Table 1. To demonstrate the amount of CPU savings, the comparison of CPU time for the analyses with and without superelement plotted against the load increment numbers is shown in Fig. 21.

As shown in Fig. 20, the predictions with and without superelement for the ultimate strength of the structure are very close. However, the computational efficiency was not significantly improved at initial load increments, since the nonlinear zone consists of one-half of the structure. Moreover, it should be noted that additional constraints from the second storey will be applied at the first storey and the second storey will play a role to sustain the structure, which results in a certain discrepancy between the models with and without superelement. This explains why a discrepancy can be found in the linear region from the models with and without superelement in Fig. 20.

To better demonstrate the efficiency improvement, an eleven-storey frame with the same material properties and cross-sectional dimensions are conducted in the next example.

Example 3: an eleven-storey frame with material yield and failure at the first two storeys

To illustrate the advantage of superelement in the analysis of localized material nonlinearity problems, the material properties and cross-sectional dimensions for both beams and columns in the previous two-storey frame example is employed to build an eleven-storey frame as shown in Fig. 22. The same loading condition shown in Fig. 17 was used again in the first storey. The numerical model and corresponding deformation are shown in Fig. 22. In the model with superelement, all elements above the first two storeys were combined as a superelement. The

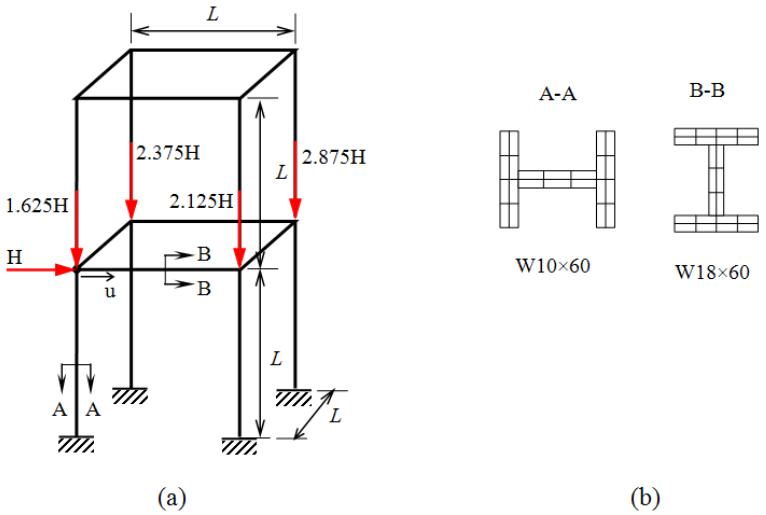

Fig. 17 Example 2: a 3D frame with material yield and failure at the first story

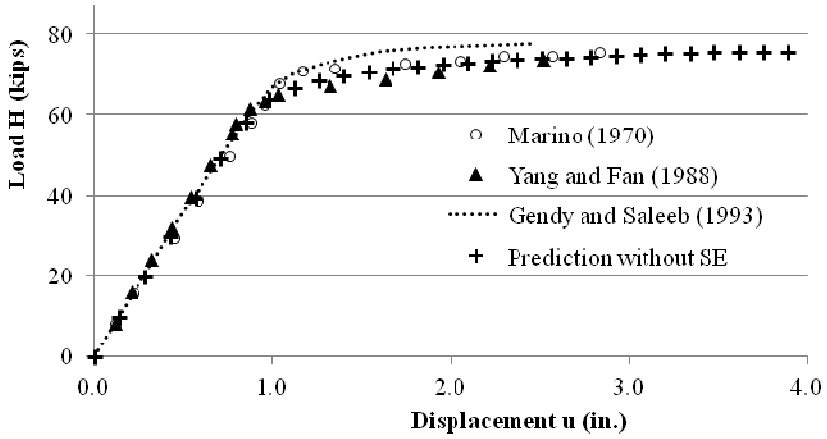

Fig. 18 Result comparisons for Example 2

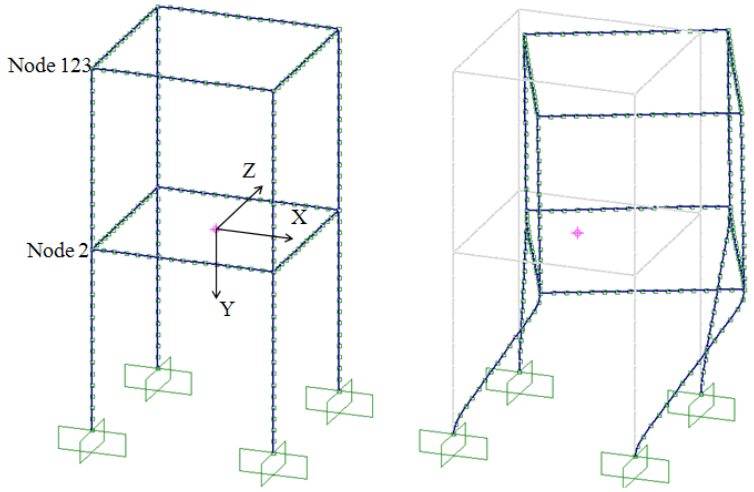

Fig. 19 Numerical model and deformation for Example 2

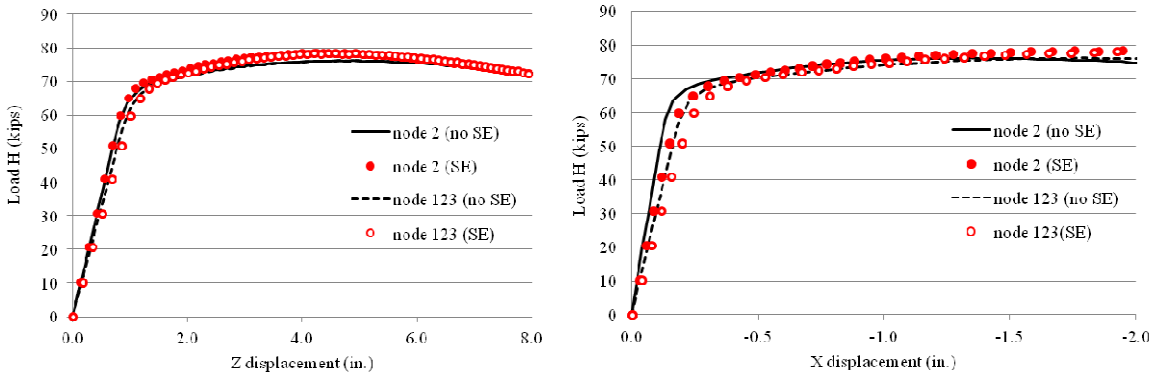

(a) *Z* direction (b) *X* direction

Fig. 20 Displacement versus loading curves for critical points in Example 2

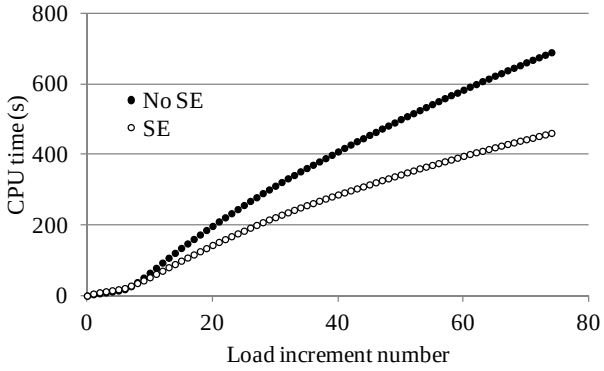

Fig. 21 CPU time comparison for Example 2 with and without superelement

Table 1 Comparisons of computational cost and CPU time for Example 2

2-storey frame	With superelement	Without superelement	Ratio (%)
No. of nodes	137	252	54.4
Computational time (s)	461.0	689.6	66.9

Table 2 Comparisons of computational cost and CPU time for Example 3

11-storey frame	With superelement	Without superelement	Ratio (%)
No. of nodes	253	1368	18.5
Computational time (s)	738.2	3390.5	21.8

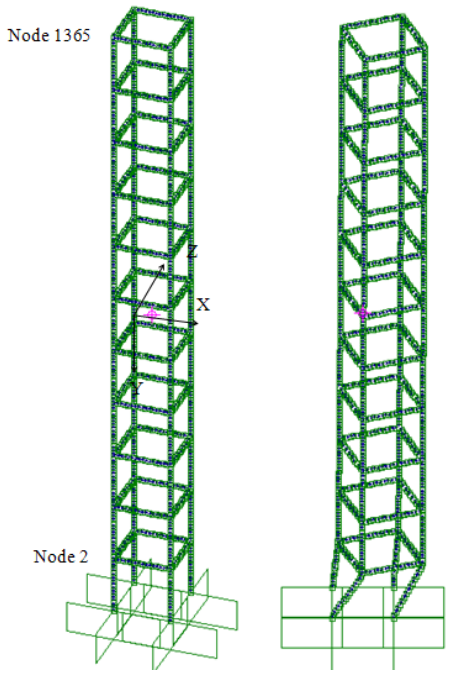

Fig. 22 Example 3: numerical model and deformation for a 3D eleven-storey frame

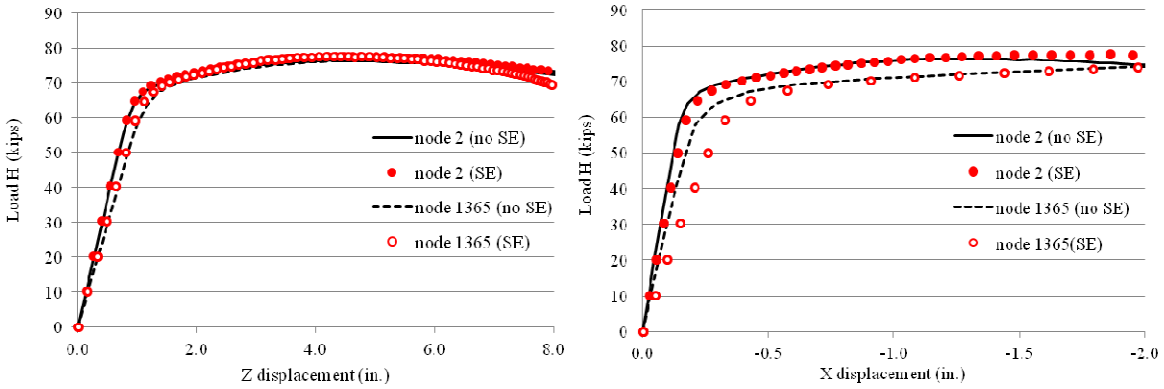

(a) *Z* direction (b) *X* direction

Fig. 23 Displacement versus loading curves for critical points in Example 3

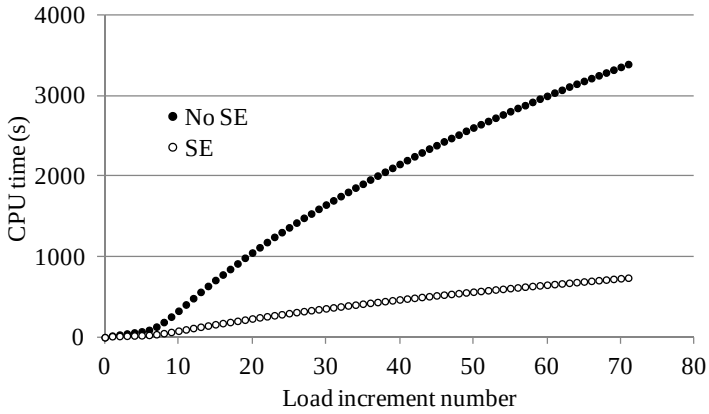

Fig. 24 CPU time comparison for Example 3 with and without superelement

displacement versus loading curves for node 2 and node 1365 are shown in Fig. 23. The comparisons of the required CPU time for the 3D eleven-storey frame is listed in Table 2. The comparison of CPU time for the models with and without superelement for different numbers of load increments is shown in Fig. 24, after the deformation in *Z* direction of node 2 achieved 8 inches.

As shown in Fig. 23, the results of predictions with and without superelement for the ultimate strength of the structure agreed well. In addition, from Fig. 24 and Table 2, it is very obvious that the superelement significantly improved the computational efficiency of the analysis. A discrepancy in results from the models with and without superelement can be seen in Fig. 23(b) and it is again due to the additional constraint on the first two storeys from the superelement above.

In Example 2 and 3, both superelements are of the second type of superelement, that is, the superelements are not directly fixed onto the foundation. To demonstrate the efficiency improvement for the first type of superelement, a 3D three-bay three-storey steel frame with the same material properties and cross-sectional dimensions are studied in Example 4, and a 2D three-storey RC frame with an exterior column removed is presented in Example 5.

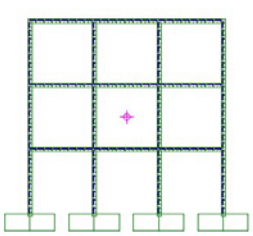

(a) Elevation view

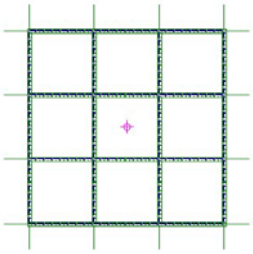

(b) Plan view

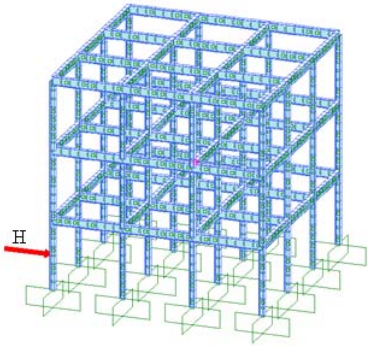

(c) Loading condition

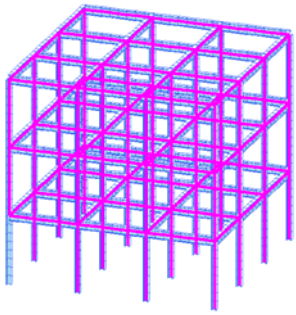

(d) Defined superelement zone (in purple)

Fig. 25 Example 4: numerical model for a 3D three-bay three-storey frame

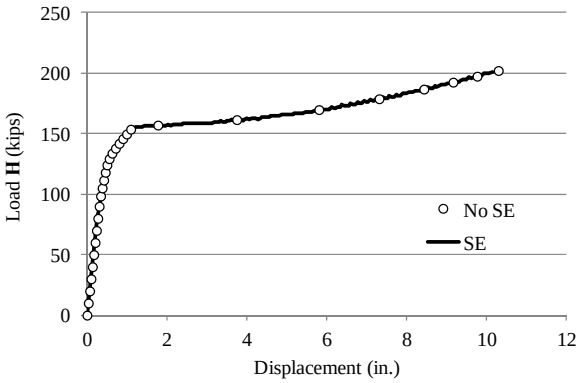

Fig. 26 Displacement versus loading curves at the loading point in Example 4

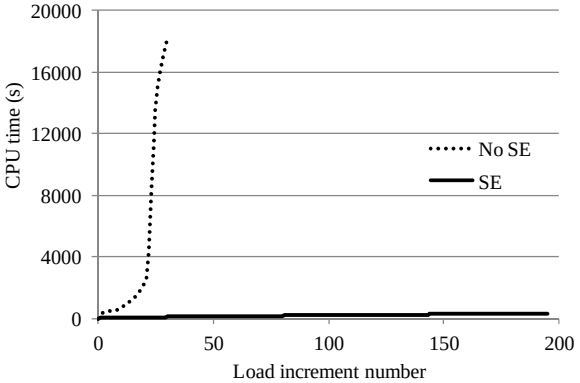

Fig. 27 CPU time comparison for Example 4 with and without superelement

Example 4: a 3D three-bay three-storey frame with a horizontal load at the first storey

The numerical model of the 3D three-bay three-storey frame is shown in Fig. 25. To avoid too much computational cost to analyze the full model without superelement, only three storeys are made in the present example. The cross-sectional dimension, material properties and element discretization for each beam and column member are the same with that in Example 2 and 3. To simulate a car bombing accident which is usually used to attack buildings by terrorists, a horizontal point load is applied at the middle point of one column at the first storey as shown in Fig. 25(c). With

Table 3 Comparisons of computational cost and CPU time for Example 4

3-bay 3-storey frame	With superelement	Without superelement	Ratio (%)
No. of nodes	18	1864	0.97
Computational time (s)	313.5	17621.0	1.78

increasing the point load, steel will yield at those elements at the loading point and at the two ends of the column. Later, the steel yielding regimes will gradually propagate to other elements of the column. Therefore, it is assumed that material nonlinearity is localized within the column and the other structural regimes remain elastic and can be defined as a superelement as shown in Fig. 25(d).

After analyzing the numerical models with and without superelement, displacement versus loading curves at the loading point are compared in Fig. 26, where good agreement is achieved before and after the material nonlinearity occurred. This means the assumption about the superelement zone is reasonable.

As shown in Fig. 27, even though different load increments in the models with and without superelement were taken to achieve the same deformation (10 in.) at the loading point, the computational time of the model with superelement is significantly decreased. To illustrate the efficiency improvement when using superelement in the numerical model, the computational cost and CPU time are listed in Table 3 as well. It can be easily seen that the efficiency of the simulation with superelement is improved tremendously.

Example 5: a 2D three-storey RC frame with an exterior column removed

As a typical progressive collapse scenario, a 2D three-storey two-bay RC frame was studied and discretized by CR beam elements as shown in Fig. 28 and the missing exterior column of the first floor represents a column loss due to a car bombing at a building corner. Three point loads were applied downwards at the top level of the numerical model. The dimensions and reinforcement details of the beams and columns are given in Fig. 28. As for the fibre model, the concrete cross-sections of beams and columns were discretized by 100 concrete fibres and each longitudinal reinforcing bar was represented by one steel fibre at the corresponding location. The employed material properties for steel and concrete are listed in Table 4, where the ratio of elongation represents the ultimate tensile strain of longitudinal reinforcement, and the given value is taken as the average of measured ultimate tensile strains by steel gauges with five times and ten times the bar diameter.

The region of the structure directly above the removed exterior column is of interest in terms of its nonlinear behaviour. Therefore, the right hand side half of the structure (highlighted in purple in Fig. 28) is treated as the linear zone and defined as a superelement. The numerical model with superelement is analyzed and the corresponding result is compared with the results based on full nonlinear analyses. Under the same value of the applied load, final deformations of the 2D three-storey RC frame with and without superelement are given in Fig. 29 which shows good agreements of the both models. The corresponding complete load-displacement responses of the two numerical models are essentially the same as shown in Fig. 30. However, it should be noted that the reason for the discrepancy of the two curves (with and without superelement) in Fig. 30 is that the material nonlinearity may have already propagated to the right half of the structure (highlighted in purple in Fig. 28), since the bar fracture occurs at the joints at the interface between

nonlinear zone and superelement zone. Therefore, the constraint on the nonlinear zone is overestimated, which can be reflected by a smaller displacement in the load-displacement responses. The numbers inside circles in Fig. 30 indicate the failure sequence as also shown in Fig. 31. It can be seen that no matter a superelement is employed or not, the same failure modes and locations can be captured. Nevertheless, the computational time for the numerical models with and without superelement is significantly different. As shown in Fig. 32, the computational time for the numerical model without superelement is more than twice as much as that with superelement.

Table 4 Material properties of reinforcing steel and concrete for Example 5

Material	Property	Measured values
Longitudinal reinforcement	Yield strength, MPa	416
	Ultimate tensile strength, MPa	526
	Ratio of elongation	25%
Lateral reinforcement	Yield strength, MPa	370
Concrete	Cylinder strength in compression, MPa	20

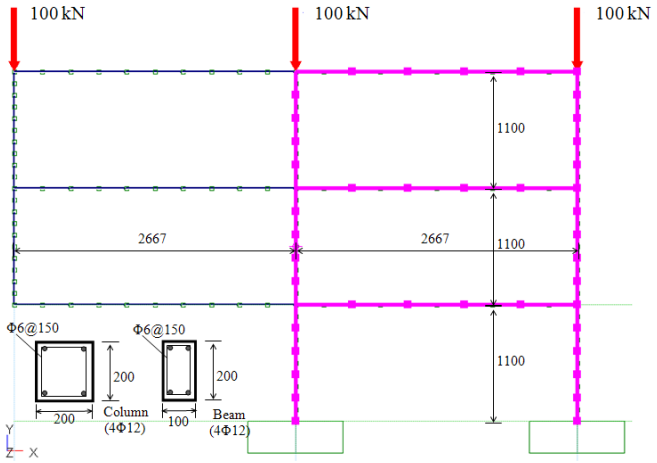

Fig. 28 Example 5: a 2D three-storey RC frame with an exterior column removed (unit in mm)

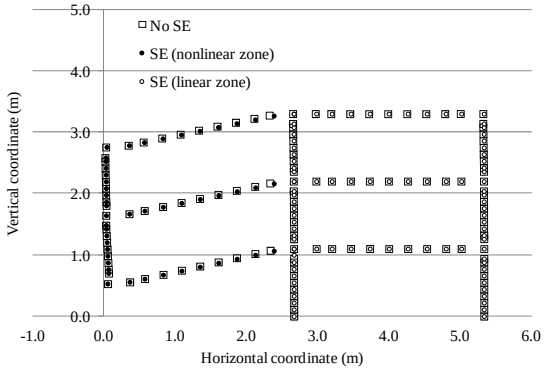

Fig. 29 Deformation of the 2D three-storey RC frame in Example 5

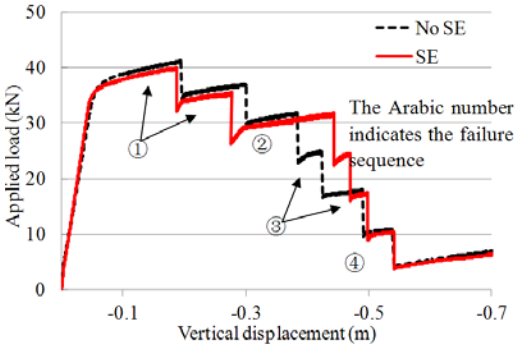

Fig. 30 Load-displacement response of the three-storey RC frame in Example 5

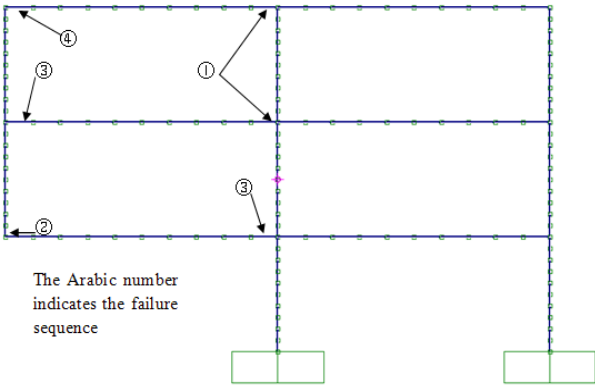

Fig. 31 Failure location and sequence of the 2D three-storey RC frame in Example 5

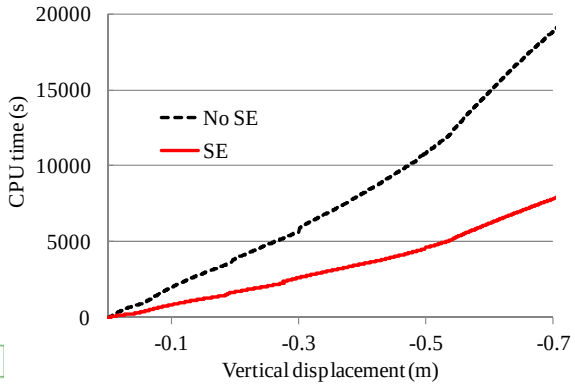

Fig. 32 Computational time comparison for Example 5 with and without superelement

5. Conclusions

In this paper, a new superelement formulation is proposed and it improves significantly the efficiency of structural deformation analysis and can be directly implemented into an existing finite element program. The numerical examples demonstrate that it can be applied to 3D multi-storey frames and gives accurate results when compared with full nonlinear analysis. However, it is noteworthy that the definition of superelement in the numerical model should be determined reasonably and can only be applied at the region with elements undergoing elastic deformation.

The improvement of computational efficiency with the superelement application will be much more obvious when a large portion of the structure is converted to the superelement zone. However, due to the preparation steps of superelement prior to the start of incremental-iterative solution, the simulation with the proposed superelement formulation may be relatively slower than the modelling without superelement in the first few increments. Nevertheless, the application of the proposed superelement formulation will be much more advantageous if a larger number of increments are applied in the nonlinear analysis.

It should be noted that the current formulation of superelement can only be applied to structural simulations with material nonlinearity localized in certain critical structural members and these regimes do not dramatically spread throughout the whole structural domain. However, the obvious limitation can be eliminated by adaptively defining the zone of superelement and such development is now under the active consideration by the authors.

Acknowledgements

This research was supported by a research grant provided by the Defence Science & Technology Agency (DSTA), Singapore, under the Protective Technology Research Centre, Nanyang Technological University, Singapore. Any opinions, findings and conclusions expressed in this paper are those of the writers and do not necessarily reflect the view of DSTA, Singapore.

References

Agrawal, O.P., Danhof, K.J. and Kumar, R. (1994), "A superelement model based parallel algorithm for vehicle dynamics", *J. Comput. Struct*., **51**(4), 411-423.

Argyris, J. (1982), "An excursion into large rotations", *Comput. Meth. Appl. Mech. Eng*., **32**(1-3), 85-155.

Bazant, Z.P. and Verdure, M. (2007), "Mechanics of progressive collapse: learning from World Trade Center and building demolitions", *J. Eng. Mech.-ASCE*, **133**, 308-319.

Belesis, S. and Labeas, G. (2010), "Development of an efficient engineering methodology for non-linear damage and post-buckling analysis of large-scale structures", *Int. J. Struct. Integr*., **1**(2), 126-139.

Belyi, M.V. (1993), "Superelement method for transient dynamic analysis of structural systems", *Int. J. Numer. Method. Eng.*, **36**(13), 2263-2286.

Cardona, A. (2000), "Superelements modelling in flexible multibody dynamics", *Multibody Syst. Dyn*., **4**(2-3), 245-266.

Cardona, A. and Geradin, M. (1991), "Modeling of superelements in mechanism analysis", *Int. J. Numer. Method. Eng*., **32**(8), 1565-1593.

Chen, S.H. and Pan, H.H. (1988), "Guyan reduction", *Commun. Appl. Numer. M*., **4**(4), 549-556.

Crisfield, M.A. (1990), "A consistent co-rotational formulation for non-linear, three-dimensional, beam-elements", *Comput. Meth. Appl. Mech. Eng*., **81**(2), 131-150.

Crisfield, M.A. (1996), *Nonlinear finite element analysis of solid and structures*, Wiley, Chinchester.

De Gersem, H., Moens, D., Desmet, W. and Vandepitte, D. (2007), "Interval and fuzzy dynamic analysis of finite element models with superelements", *J. Comput. Struct*., **85**(5-6), 304-319.

Dvorkin, E.N., Onte, E. and Oliver, J. (1988), "On a non-linear formulation for curved Timoshenko beam elements considering large displacement/rotation increments", *Int. J. Numer. Method. Eng*., **26**(7), 1597-1613.

Gendy, A.S. and Saleeb, A.F. (1993), "Generalized yield surface representations in the elasto-plastic three-dimensional analysis of frames", *J. Comput. Struct*., **49**(2), 351-362.

Hartmann, D. *et al*. (2008), "Structural collapse simulation under consideration of uncertainty - Fundamental concept and results", *J. Comput. Struct*., **86**(21-22), 2064-2078.

Huang, S.J. and Li, P.Z. (2010), "Superelement method based structure simulation of large pallet structure", *Second International Conference on Computer Engineering and Applications*.

Jacobsen, K.P. (1983), "Fully integrated superelements: a database approach to finite element analysis", *J. Comput. Struct*., **16**(1-4), 307-315.

Ju, F. and Choo, Y.S. (2005), "Super element approach to cable passing through multiple pulleys", *Int. J. Solids Struct.*, **42**(11-12), 3533-3547.

Kim, H.S., Lee, D.G. and Kim, C.K. (2005), "Efficient three-dimensional seismic analysis of a high-rise building structure with shear walls", *Eng. Struct*., **27**(6), 963-976.

Li, Z.X. (2007), "A co-rotational formulation for 3D beam element using vectorial rotational variables", *Comput. Mech*., **39**(3), 309-322.

Long, X., *et al*. (2012). "A 3D co-rotational beam element with geometric and material nonlinearities for steel and RC framed structures", *4th International Conference on Design and Analysis of Protective Structures*, Jeju, Korea.

Maressa, A., Mundo, D., Donders, S. and Desmet, W. (2011), "A wave-based substructuring approach for concept modeling of vehicle joints", *J. Comput. Struct*., **89**(23-24), 2369-2376.

Marino, S. (1970), "Analysis of space frames", Thesis presented to Lehigh University, Bethlehem, PA., in partial fulfillment of the requirements for the degree of Doctor of Philosophy.

National Institute of Standards and Technology (2005), Federal building and fire safety investigation of the world trade center disaster: Final report on the collapse of the world trade center building 7 (draft for public comment).

Przemieniecki, J.S. (1968), *Theory of matrix structural analysis*, Mc Graw-Hill Publication, New York.

Qiu, K.P., Zhang, W.H., Domaszewski, M. and Chamoret, D. (2009), "Topology optimization of periodic

cellular solids based on a superelement method", *Eng. Optimiz*., **41**(3), 225-239.
Steenbergen, R.D.J.M. (2007), "Super elements in high-rise buildings under stochastic wind load", PhD Thesis, Delft University of Technology.
Unified Facilities Criteria (UFC)-DoD (2005), Design of buildings to resist progressive collapse, Department of Defense.
Wilson, E.L. (1974), "The static condensation algorithm", *Int. J. Numer. Method. Eng*., **8**(1), 198-203.
Yang, Y.B. and Fan, H.T. (1988), "Yield surface modeling of I-sections with nonuniform torsion", *J. Eng. Mech.-ASCE*, **114**(6), 953-972.
Yuan, W. and Tan, K.H. (2011), "Modeling of progressive collapse of a multi-storey structure using a spring-mass-damper system", *Struct. Eng. Mech.*, **37**(1), 79-93.
Zemer, D.T. (1979). "Implementation of superelement analysis at the production level", *Proceeding of the MSC/NASTRAN Users' Confrence*.

Notations

$\mathbf{e}_x$, $\mathbf{e}_y$, $\mathbf{e}_z$ = local nodal vectors of the connecting node in the global system
E = Young's modulus
G = shear modulus
$\mathbf{F}$ = internal nodal force at connecting nodes
$\mathbf{M}$ = internal nodal moment at connecting nodes
$\mathbf{K}_s$ = stiffness matrix of the superelement
$\mathbf{K}_{ns}$ = non-superelement stiffness matrix
L = geometry dimension
P = external load
$\mathbf{P}_s$ = external load within the superelement zone
$\mathbf{R}$ = orthogonal rotation matrix
$\mathbf{R}_i$ = rigid-body rotation matrix at connecting node i
$\mathbf{S}$ = skew-symmetric matrix
$\boldsymbol{u}$ = the nodal displacement
$\boldsymbol{u}_L$ = relative deformation of superelement with respect to the nonlinear zone
$\boldsymbol{u}_G$ = superelement deformation in the global coordinate system
${}^0\boldsymbol{U}\sim{}^6\boldsymbol{U}$ = deformation components when forming stiffness matrix of superelement
λ = arbitrary nonzero factor
θ_1, θ_2, θ_3 = rotational variables of the connecting node
σ_y = yield strength
$\boldsymbol{\omega}$ = pseudo-vector of the natural rotation